Magnetic excitations in the noncentrosymmetric magnet $Sr_2MnSi_2O_7$

Masahiro Kawamata,[1] Xiaoqi Pang,[1] Hiroshi Murakawa,[2] Seiko Ohira-Kawamura,[3] Kenji Nakajima,[3] Hidetoshi Masuda,[4] Masaki Fujita,[4] Noriaki Hanasaki,[2] Yoshinori Onose,[4] and Yusuke Nambu[4,5,6]

[1]*Department of Physics, Tohoku University, Sendai, Miyagi 980-8578, Japan*
[2]*Department of Physics, Osaka University, Toyonaka, Osaka 560-0043, Japan*
[3]*Materials and Life Science Division, J-PARC Center, Japan Atomic Energy Agency, Tokai, Ibaraki 319-1195, Japan*
[4]*Institute for Materials Research, Tohoku University, Sendai, Miyagi 980-8577, Japan*
[5]*Organization for Advanced Studies, Tohoku University, Sendai, Miyagi 980-8577, Japan*
[6]*FOREST, Japan Science and Technology Agency, Kawaguchi, Saitama 332-0012, Japan*

(Received 29 October 2024; accepted 2 January 2025; published 22 January 2025)

Magnetic excitations in the noncentrosymmetric magnet $Sr_2MnSi_2O_7$ were investigated through inelastic neutron scattering measurements. Major magnetic excitations are limited up to the energy transfer of 0.5 meV, and two magnon branches under zero magnetic field were well explained in the framework of linear spin-wave theory. The magnitudes of the square-lattice in-plane and interplane nearest-neighbor interactions, spin anisotropy term, and the Dzyaloshinskii-Moriya interaction are, respectively, estimated to be $J_1 = 45.54(5)$ μeV, $J_2 = 0.52(1)$ μeV, $\Lambda = 4.98(11)$ μeV, $D_{xy} = 0.02(9)$ μeV, and $D_z = 4.10(1)$ μeV, and calculations using these parameters reproduce experimental data quite well. $Sr_2MnSi_2O_7$ appears to have the smallest energy scale among the melilite-type compounds, and the small $J_2/J_1 = 0.0114(2)$ indicates the strong two dimensionality.

DOI: 10.1103/PhysRevMaterials.9.014407

I. INTRODUCTION

Multiferroics, in which magnetism and dielectricity are cross correlated are expected to be one of the key ingredients for developing power-saving devices [1]. Spin-induced multiferroics, as first identified in $TbMnO_3$ [2], have an advantage of electrical/magnetic mutual correlation and exemplified an easy control of electric charge by magnetic signals and magnetization by electric currents [3]. Spin-induced dielectricity is classified into three major mechanisms: exchange striction [4], spin current [5], and spin-dependent d-p hybridization [6].

Melilite-type compounds are one of the representative groups with multiferroic properties in the d-p hybridization mechanism [7]. The compounds with the stoichiometry $A_2MB_2X_7$ (A = Ca, Sr, Ba, M = Mn, Co, Cu, B = Si, Ge, X = O, S) [8–18] have generally the $P\bar{4}2_1m$ space group and the Dzyaloshinskii-Moriya (DM) interaction inherent owing to the broken inversion symmetry. The competition between the antiferromagnetic nearest-neighbor exchange interaction and the DM interaction naturally yields canting antiferromagnetic structures [11,19] and even helical magnetic structures [20]. The d-p hybridization induced by MX_4 tetrahedra leads to a spin direction-dependent dielectricity that can easily be controlled by external magnetic fields [21]. Besides that, melilite-type compounds are of broad interest for circular dichroism [22], quantum fluctuations [23], giant optical effects [24], and magnon textures [25].

The melilite-type compounds possess a wide variety of magnetic structures. The compound with $M = Co^{2+}$ has the C-type antiferromagnetic structure, and the magnetic moment is projected onto the ab plane [11,19,26]. On the other hand, for $M = Mn^{2+}$, magnetic structures are ranged from the C-type ($Ba_2MnSi_2O_7$ [27]) to the G-type ($Ba_2MnGe_2O_7$ [28–30], $Sr_2MnGe_2O_7$ [26]), which have magnetic moments either on the ab plane or along the c axis. The model spin Hamiltonian is also M cation dependent, where the XXZ model taking into account anisotropic exchange interaction [31,32] describes $M = Co^{2+}$ ($S = 3/2$) cases, whereas a Heisenberg-type exchange interaction [33] is employed for $M = Mn^{2+}$ ($S = 5/2$). To achieve a collective understanding of the magnetism of the melilite-type compounds, information on the magnetic structure and excitations over separate mixtures of A, B, and X atoms is required.

We here measure magnetic excitations of a new melilite-type compound, $Sr_2MnSi_2O_7$, and then determine the effective model for this particular material. $Sr_2MnSi_2O_7$ has a two-dimensional (2D) network of MnO_4 and SiO_4 tetrahedra as illustrated in Figs. 1(a) and 1(b). Mn^{2+} ions with spin $S = 5/2$ reside on a square lattice on the ab plane [34], which is stacked along the c axis and is separated by Sr^{2+} ions. An antiferromagnetic order appears below $T_N = 3.4$ K [35], and the G-type canting antiferromagnetic structure is refined [36]. The magnetic structure is represented by the magnetic space group $Cmc2_1.1'_c$ with the magnetic wave vector $\vec{q}_m = (0, 0, 1/2)$ r.l.u. The in-plane weak ferromagnetic components are oriented toward [110], and the magnetic moments are stacked antiparallel between the planes [Figs. 1(c) and 1(d)]. Prior to verifying the multiferroic properties of the compound and possible magnon texture, it is crucial to construct an effective microscopic model. In this study, we observe two magnon modes in $Sr_2MnSi_2O_7$ through an inelastic neutron scattering experiment with zero magnetic field. The observed magnon

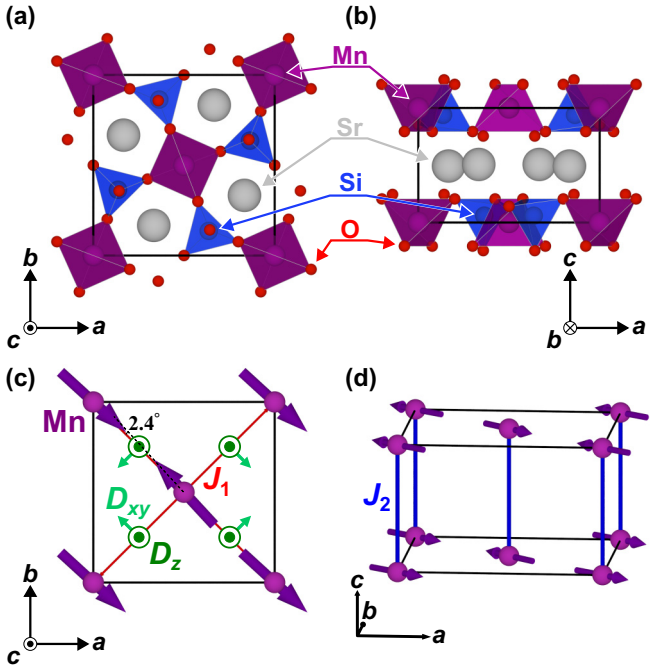

FIG. 1. Crystal structure of $Sr_2MnSi_2O_7$ projected onto (a) the *ab* plane and (b) the *ac* plane. The canted antiferromagnetic structure and interaction pathways are shown in (c) the *ab* and (d) the bird's eye view.

spectra are well accounted for by the linear spin-wave theory, and the strengths of primary magnetic interactions are refined.

II. EXPERIMENT

Polycrystalline samples of $Sr_2MnSi_2O_7$ were synthesized by the solid-state reaction. Single-crystalline samples were then grown in the air by the floating zone method using an image furnace [7]. A single crystal with a cylindrical shape was obtained, and it was cut to the size $\phi 5 \times 30$ mm^3 for neutron measurements. The sample mass was approximately 1.6 g, with a mosaicity estimated to be 0.38(1)°. The quality of the obtained samples was confirmed by x-ray diffraction and neutron diffraction [36] measurements.

To observe magnetic excitations in $Sr_2MnSi_2O_7$, an inelastic unpolarized neutron scattering experiment was carried out on the chopper spectrometer BL14 AMATERAS [37] at J-PARC, Japan. The instrument enables effective data collection using the multiple incident energies (E_i) simultaneously. We employed $E_i = 7.733, 3.136, 1.687$ meV with energy resolutions of 0.273, 0.073, 0.027 meV at the elastic position, respectively. The crystal oriented on the $[HK0]$ horizontal scattering zone, was inserted into the instrument-equipped cryostat without applying magnetic fields. No background subtraction was performed, and the observed intensity was normalized by the number of protons.

III. RESULTS AND DISCUSSION

Overall magnetic excitations measured at 1.91(4) K using $E_i = 3.136$ meV under zero magnetic field are depicted in Fig. 2(a), where the whole excitations reside below the energy

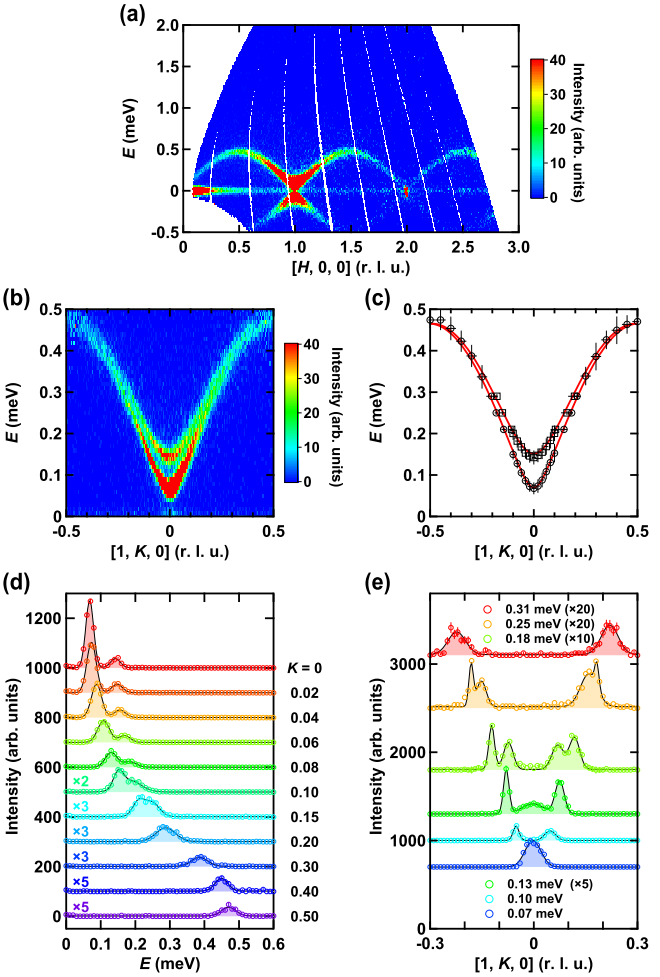

FIG. 2. (a) Neutron intensity map for the $[H, 0, 0]$ r.l.u. direction using $E_i = 3.136$ meV and (b) enlarged map for the $[1, K, 0]$ r.l.u. direction using $E_i = 1.687$ meV. (c) Estimated peak positions of magnon spectra from [(d),(e)], with red curves giving the fit based upon the linear spin-wave calculation. (d) One-dimensional cut along the E where the K integration is ± 0.01 r.l.u. and $0.09 \leqslant H \leqslant 1.01$ r.l.u., together with fits using Gaussian peaks. The observed neutron-scattering intensity was multiplied for data with $K \geqslant 0.10$ to enlarge the observed peak. (e) One-dimensional cut along $[1, K, 0]$ r.l.u. direction where the constant E integration is ± 0.005 meV and $0.09 \leqslant H \leqslant 1.01$, $-0.1 \leqslant L \leqslant 0.1$ r.l.u.

transfer, $E = 0.5$ meV. Incoherent scattering centered at $E = 0$ meV is visible yet very small reflecting the small incoherent scattering cross sections of Sr (0.06 barn), Mn (0.4 barn), Si (0.004 barn), and O (0.0008 barn) [38]. The magnon dispersion using $E_i = 1.687$ meV with a tighter energy resolution is shown in Fig. 2(b), where two distinct branches are clearly observed. K-integrated one-dimensional data along E are derived and are fit by Gaussian peaks [Fig. 2(d)]. Two peaks are observed for smaller K regime, and they merge into a single peak with increasing K. The cut data along the K direction [Fig. 2(e)] are also analyzed, and estimated peak positions are summarized in Fig. 2(c).

To evaluate exchange interactions, spin anisotropy term and the DM interaction, obtained data were analyzed within the linear spin-wave calculation. The spin Hamiltonian we

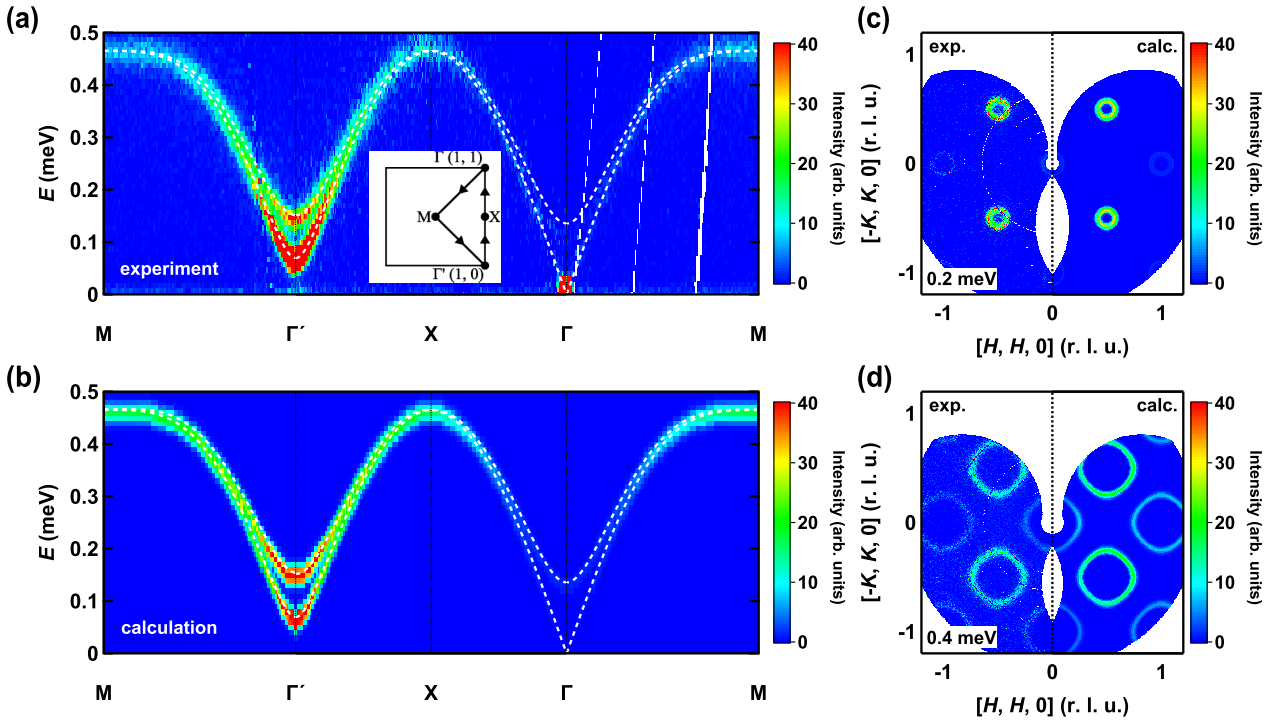

FIG. 3. (a) Observed and (b) calculated neutron intensity map of $Sr_2MnSi_2O_7$ along high-symmetry directions. Measurements are performed at $T = 1.91(4)$ K ($< T_N$), and data were integrated for $-0.1 \leqslant L \leqslant 0.1$ r.l.u. and over a thickness of ± 0.005 r.l.u. perpendicular to the path directions. The inset to (a) draws the $[HK0]$-reciprocal space map. Constant energy slices for (c) $0.19 \leqslant E \leqslant 0.21$ meV and (d) $0.39 \leqslant E \leqslant 0.41$ meV are compared with the corresponding calculations.

employed reads,

$$\mathcal{H} = \sum_{\langle i,j \rangle} J_1 \vec{S}_i \cdot \vec{S}_j + \sum_{\langle k,l \rangle} J_2 \vec{S}_k \cdot \vec{S}_l + \sum_i \Lambda (\vec{S}_i^z)^2 + \sum_{\langle i,j \rangle} \vec{D} \cdot (\vec{S}_i \times \vec{S}_j), \quad (1)$$

where, i, j, k, l indices stand for Mn^{2+} at the Wyckoff $2a$ site, $\langle i, j \rangle$ and $\langle k, l \rangle$ run nearest-neighbor pairs on the ab plane and along the c axis, respectively [corresponding pathways depicted in Figs. 1(c) and 1(d)]. Λ is the spin anisotropy term, and $\Lambda > 0$ corresponds to the easy-plane anisotropy. The DM interaction $\vec{D} = D_{xy} \frac{\vec{e}_x + \vec{e}_y}{\sqrt{2}} + D_z \vec{e}_z$ is allowed reflecting the noncentrosymmetric space group [Fig. 1(c)].

First, assuming sufficiently small $|\vec{D}|$, we consider a collinear magnetic structure with magnetic moments along [110]. By diagonalizing the Hamiltonian in Eq. (1) with $\vec{D} = 0$, we obtain the magnon energy dispersion $\varepsilon(\vec{Q})$ with $\vec{Q} = (Q_x, Q_y, Q_z)$ r.l.u. as follows,

$$\varepsilon(\vec{Q}) = S\Big\{(4J_1 + 2J_2 + \Lambda)^2 - \big(4J_1 \cos \pi Q_x \cos \pi Q_y + 2J_2 \cos 2\pi Q_z \pm \Lambda\big)^2\Big\}^{\frac{1}{2}}. \quad (2)$$

The eigenenergies $(\varepsilon_1, \varepsilon_2)$ can analytically be derived at high-symmetry points such as $\vec{Q}^X = (1/2, 0, 0)$ and $\vec{Q}^{\Gamma'} = (1, 0, 0)$ r.l.u.,

$$\varepsilon_1^X = 2S\sqrt{2(J_1 + J_2)(2J_1 + \Lambda)}, \quad (3)$$

$$\varepsilon_2^X = 2S\sqrt{2J_1(2J_1 + 2J_2 + \Lambda)}, \quad (4)$$

$$\varepsilon_1^{\Gamma'} = 2S\sqrt{2J_2(4J_1 + \Lambda)}, \quad (5)$$

$$\varepsilon_2^{\Gamma'} = 2S\sqrt{4J_1(2J_2 + \Lambda)}. \quad (6)$$

Given $J_2 \ll J_1$ in $Sr_2MnSi_2O_7$ as discussed later on, $\varepsilon_1^X \simeq \varepsilon_2^X$ holds and they can be approximated as $2S\sqrt{2J_1(2J_1 + \Lambda)}$. As Eqs. (5) and (6) formulate, the presence of J_2 results in energy-gap formation at $\vec{Q}^{\Gamma'} = (1, 0, 0)$ r.l.u., whereas Λ helps in lifting the degeneracy. Through fits to the obtained data [Fig. 2(d)], corresponding eigenenergies are experimentally estimated as $\varepsilon_1^X \simeq \varepsilon_2^X = 0.47(2)$ meV, $\varepsilon_1^{\Gamma'} = 0.07(1)$ meV, and $\varepsilon_2^{\Gamma'} = 0.14(2)$ meV. The strengths of the magnetic interactions were then numerically obtained using the random swarm optimization method [39] by fit to experimental data for whole momentum transfer, $\vec{Q}$ space measured, which nicely converges and gives $J_1 = 45.28(5)$ μeV, $J_2 = 0.52(1)$ μeV, and $\Lambda = 3.95(14)$ μeV. Using these values, the eigenenergies are computed as $\varepsilon^X = 0.4625(5)$ meV, $\varepsilon_1^{\Gamma'} = 0.0694(7)$ meV, and $\varepsilon_2^{\Gamma'} = 0.1503(2)$ meV, yielding fair agreement with analytical solutions. These parameters can nicely reproduce the experimental data as depicted in Fig. 2(c).

Using the obtained parameters, we calculate the magnon spectra in the same dynamic range as measured in Fig. 3(a). Figure 3(b) gives results that are almost completely in accordance with our experimental findings. Magnetic excitations at constant energies are also compared in Figs. 3(c) and 3(d).

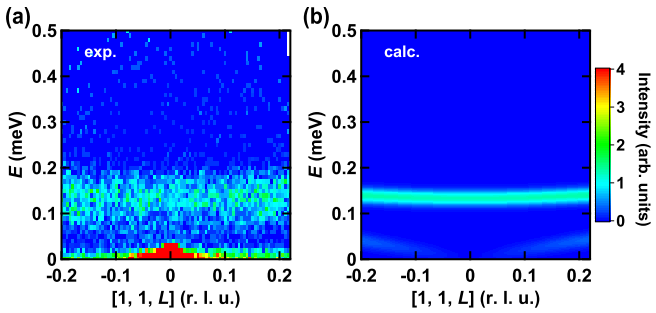

FIG. 4. (a) Observed and (b) calculated neutron intensity map of $Sr_2MnSi_2O_7$ along [1, 1, L] r.l.u. Measurements were performed using $E_i = 1.687$ meV, and data were integrated for $0.9 \leqslant H \leqslant 1.1$ r.l.u. and $0.9 \leqslant K \leqslant 1.1$ r.l.u.

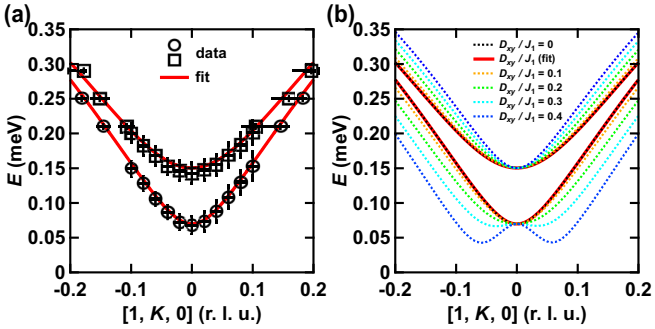

FIG. 5. (a) Estimated peak positions, which are identical to Fig. 2(c), and fit results using Eq. (1). (b) Simulated magnon branches for changing D_{xy}/J_1 for 0.0–0.4 (dashed curves), where fit results give the solid red curve [$D_{xy} = 0.02(9)$; $D_{xy}/J_1 = 0.4(2.0) \times 10^{-4}$].

With increasing E, magnon branches spread while holding $\bar{4}$ symmetric shapes. Such high reproducibility of experimental data validates our parametrizations.

Figure 4(a) shows magnon spectra along the [1, 1, L] direction. Since the *ab* plane was on the horizontal scattering plane and the detector coverage along the perpendicular direction (c) is quite limited, data for $-0.2 \lesssim L \lesssim 0.2$ r.l.u. were only obtained. In Fig. 4(a), allowed nuclear reflection at (1,1,0) is visible, and a weak magnetic signal was observed between 0.1 and 0.2 meV. Our calculation [Fig. 4(b)] can roughly reproduce the experimental data including the dispersionless magnon branch reflecting the small J_2. However, the experimental data clearly have a rather broad spread along E than the calculation. This may be due to unmeeting the decent scattering condition and/or capturing some peculiar dynamics, and further measurements on [$H0L$] or [HHL] zones are thus future perspectives.

Among the above-mentioned refined parameters, $J_1 > 0$ and $J_2 > 0$ stand for antiferromagnetic interactions for the intra- and interplanes. This stabilizes the G-type antiferromagnetic structure being the same as in $Sr_2MnGe_2O_7$ and $Ba_2MnGe_2O_7$ [26,33]. The magnetic interactions of $Sr_2MnSi_2O_7$ are slightly smaller than $Ba_2MnGe_2O_7$ with $J_1 = 55.6(6)$ μeV and $J_2 = 2.0(2)$ μeV [33]. The values of J_2/J_1 are 0.0114(2) and 0.036(4) for $Sr_2MnSi_2O_7$ and $Ba_2MnGe_2O_7$, respectively. The smaller J_2/J_1 indicates that $Sr_2MnSi_2O_7$ has much stronger two dimensionality than $Ba_2MnGe_2O_7$.

We now move on to the spin anisotropy term Λ. In $M = Co^{2+}$ systems among the melilite-type compounds, unquenched orbital degree of freedom is evidenced by the temperature-dependent susceptibility [12], leading to three orders of magnitude larger spin anisotropy, such as $\Lambda = 1.034$ meV for $Ba_2CoGe_2O_7$ [31]. On the other hand, in $M = Mn^{2+}$ systems, Λ stays in μeV orders reflecting the isotropic spin as $\Lambda = 2.06$ μeV for $Ba_2MnGe_2O_7$ [29]. The weak easy-plane anisotropy is owing to magnetic dipole-dipole interaction [40], and in fact, the magnetization process behaves weakly anistropic [35].

Next, by turning $\vec{D}$ on, the magnetic structure is no longer of collinear. The c component of the DM interaction, D_z, competes with J_1 and then stabilizes a canted antiferromagnetic structure. With nearest-neighbor spins $\vec{S}_1$, $\vec{S}_2$ and their interactions J_1, D_z, the internal energy is written as follows,

$$E = J_1 \vec{S}_1 \cdot \vec{S}_2 + D_z(\vec{S}_1 \times \vec{S}_2)_z. \quad (7)$$

By minimizing this energy, a relationship between D_z/J_1 and θ being the canting angle can be derived as $|\theta| = \frac{1}{2}\tan^{-1} D_z/J_1$. Recent magnetic structure study has refined that $Sr_2MnSi_2O_7$ has $D_z/J_1 = 0.09$ with $\theta \sim 2.4^\circ$ from powder diffraction data [36]. Given that the estimation was made via the spherically $\vec{Q}$ integration and four sorts of domain formations exist, $D_z/J_1 = 0.09$ thus poses the lower minimum. The *ab* component of the DM interaction, D_{xy}, makes off-diagonal components finite in the spin Hamiltonian, affecting the magnon dispersion shapes at reciprocal places away from the Γ points. Using the fixed $D_z/J_1 = 0.09$ and variable D_{xy}, further numerical fit was performed, and obtained results are $J_1 = 45.54(5)$ μeV, $J_2 = 0.52(1)$ μeV, $\Lambda = 4.98(11)$ μeV, $D_{xy} = 0.02(9)$ μeV, $D_z = 4.10(1)$ μeV [Fig. 5(a)]. As simulated in Fig. 5(b), with increasing D_{xy}, the lower-energy magnon dispersion should have two local minima [41]. Note that the evaluated D_{xy} under zero field appears to be negligibly small reflecting the presence of the four sorts of magnetic domains averaging out the asymmetry of the dispersion. Our analysis on the peak spread along $\vec{Q}$ at (1,0,0) poses the upper maximum, $D_{xy}/J_1 \lesssim 0.28$. Experiments under finite fields will be needed to precisely determine D_{xy}.

We here compare the inplane nearest-neighbor exchange interaction J_1 and the whole excitation energies (Table I). Again $Sr_2MnSi_2O_7$ has $J_1 = 45.5$ μeV, whereas $J_1 = 55.6$ μeV [33,42] for $Ba_2MnGe_2O_7$, $J_1 = 208$ μeV [12,31] for $Ba_2CoGe_2O_7$, and $J_1 = 150$ μeV [43] for $Ba_2FeSi_2O_7$. Interestingly, $M = Mn^{2+}$ systems with the largest S have smaller J_1 values than the Co^{2+} and Fe^{2+} cases. As Eqs. (3) and (4) formulate, the whole energy scale, i.e., the upper maximum at the zone boundary ($\vec{Q}^X$), is S-size dependent. Experimentally determined upper maximum in $Sr_2MnSi_2O_7$ is 0.5 meV, which is comparable with 0.6 meV for $Ba_2MnGe_2O_7$ [33] but is quite smaller than 2 meV for $Ba_2CoGe_2O_7$ [31] and 2.5 meV for $Ba_2FeSi_2O_7$ [44]. The fact is owing to the small J_2 and Λ in $Sr_2MnSi_2O_7$, and the target compound turns out to have the smallest energy scale among the melilite-type compounds with known strengths of the magnetic interactions.

TABLE I. The magnetic transition temperature, magnetic wave vector, interaction constants, and superexchange angles are summarized for several melilite-type compounds.

Compound	T_N (K)	$\vec{q}_m$ (r.l.u.)	J_1 (μeV)	J_2 (μeV)	Λ (μeV)	$\angle M$-O-O_{intra} (°)	$\angle M$-O-O_{inter} (°)	Ref.
$Sr_2MnSi_2O_7$	3.4	(0,0,1/2)	45.54(5)	0.52(1)	4.98(11)	141.34(8)	92.40(7)	this study & [36]
$Ba_2MnGe_2O_7$	4.0	(0,0,1/2)	55.6(6)	2.0(2)	2.06(7)	141.73(3)	93.97(2)	[29,33]
$Ba_2FeSi_2O_7$	5.2	(0,0,1/2)	150	2.5	1400	144.57(11)	90.35(8)	[43]
$Ba_2CoGe_2O_7$	6.7	(0,0,0)	$J_{xx} = 208, J_{zz} = 253$		1034	142.17(5)	95.20(4)	[11,31]

To more closely examine magnetic interactions compared with the sibling $Ba_2MnGe_2O_7$, superexchange pathways are examined. In the melilite-type compounds, superexchange pathways for J_1 and J_2 require electron hopping via two oxygens like Mn-O-O-Mn, and we use the structural parameters refined at 10 K [28,36]. For J_1 within the plane, bond angles are 141.34(8)° for $Sr_2MnSi_2O_7$ and 141.73(3)° for $Ba_2MnGe_2O_7$. For J_2 in interplane, on the other hand, bond angles are 92.40(7)° for $Sr_2MnSi_2O_7$ and 93.97(2)° for $Ba_2MnGe_2O_7$. The differences in these angles fall within a few degrees, yet yielding more than 18% differences in J_1 and J_2. Besides that, the Kanamori-Goodenough rule [45,46] predicts that interactions are antiferromagnetic and ferromagnetic when the bond angles are close enough to 180° and 90°, respectively. However, this is not the case for both compounds given both J_1 and J_2 are antiferromagnetic. The difference in the magnetic interactions may be due to variations of the wave function overlaps reflecting separate ionic radii. The first-principles calculations succeeded in qualitatively explaining the difference of the interactions between $Sr_2MnSi_2O_7$ and $Ba_2MnGe_2O_7$ [40]. Our refined parameters of magnetic interactions would help enhance the accuracy of calculations.

IV. CONCLUSIONS

To summarize, we observed the magnon spectra of the noncentrosymmetric antiferromagnet $Sr_2MnSi_2O_7$ through the inelastic neutron scattering experiment on a single-crystalline sample. Through the analyses of magnetic excitations up to 0.5 meV, the primary magnetic interactions are successfully refined based upon the linear spin-wave theory, and the experimental data are actually well reproduced using such parameters. The target compound stays at the smallest energy scale among the melilite-type compounds, and the tiny J_2/J_1 implies the strong inherent two dimensionality.

ACKNOWLEDGMENTS

We thank T. Arima, H. Kawamura, and T. Koretsune, J. Nasu, K. Ohgushi for their valuable discussions. This work was supported by the JSPS (Grants No. JP22KJ0312, No. JP21H03732, No. JP22H05145, No. JP24K00572, No. JP24H01638, and No. JP24H00189), FOREST (Grant No. JPMJFR202V) and SPRING from JST, and the Graduate Program in Spintronics at Tohoku University. Work at J-PARC was performed under the user program (No. 2020B0105).

[1] M. Fiebig, T. Lottermoser, D. Meier, and M. Trassin, Nat. Rev. Mat. **1**, 16046 (2016).
[2] T. Kimura, T. Goto, H. Shintani, K. Ishizaka, T. Arima, and Y. Tokura, Nature (London) **426**, 55 (2003).
[3] Y. Tokura, S. Seki, and N. Nagaosa, Rep. Prog. Phys. **77**, 076501 (2014).
[4] N. Hur, S. Park, P. A. Sharma, J. S. Ahn, S. Guha, and S.-W. Cheong, Nature (London) **429**, 392 (2004).
[5] H. Katsura, N. Nagaosa, and A. V. Balatsky, Phys. Rev. Lett. **95**, 057205 (2005).
[6] T. Arima, J. Phys. Soc. Jpn. **76**, 073702 (2007).
[7] H. Murakawa, Y. Onose, S. Miyahara, N. Furukawa, and Y. Tokura, Phys. Rev. B **85**, 174106 (2012).
[8] A. Sazonov, V. Hutanu, M. Meven, G. Roth, I. Kézsmárki, H. Murakawa, Y. Tokura, and B. Náfrádi, Acta Cryst. B **72**, 126 (2016).
[9] H. T. Yi, Y. J. Choi, S. Lee, and S.-W. Cheong, Appl. Phys. Lett. **92**, 212904 (2008).
[10] V. Hutanu, A. Sazonov, H. Murakawa, Y. Tokura, B. Naáfraádi, and D. Chernyshov, Phys. Rev. B **84**, 212101 (2011).
[11] V. Hutanu, A. Sazonov, M. Meven, H. Murakawa, Y. Tokura, S. Bordács, I. Kézsmárki, and B. Náfrádi, Phys. Rev. B **86**, 104401 (2012).
[12] V. Hutanu, A. P. Sazonov, M. Meven, G. Roth, A. Gukasov, H. Murakawa, Y. Tokura, D. Szaller, S. Bordács, I. Kézsmárki, V. K. Guduru, L. C. J. M. Peters, U. Zeitler, J. Romhányi, and B. Náfrádi, Phys. Rev. B **89**, 064403 (2014).
[13] I. V. Solovyev, Phys. Rev. B **91**, 224423 (2015).
[14] A. Sazonov, M. Meven, G. Roth, R. Georgii, I. Kézsmárki, V. Kocsis, Y. Tokunaga, Y. Taguchi, Y. Tokura, and V. Hutanu, J. Appl. Cryst. **49**, 556 (2016).
[15] M. Akaki, H. Iwamoto, T. Kihara, M. Tokunaga, and H. Kuwahara, Phys. Rev. B **86**, 060413(R) (2012).
[16] M. Akaki, D. Yoshizawa, A. Okutani, T. Kida, J. Romhányi, K. Penc, and M. Hagiwara, Phys. Rev. B **96**, 214406 (2017).
[17] R. Kurihara, Y. Sato, A. Miyake, M. Akaki, K. Mitsumoto, M. Hagiwara, H. Kuwahara, and M. Tokunaga, Phys. Rev. B **109**, 125129 (2024).
[18] T. Endo, Y. Doi, M. Wakeshima, K. Suzuki, Y. Matsuo, K. Tezuka, T. Ohtsuki, Y. J. Shan, and Y. Hinatsu, Inorg. Chem. **56**, 2459 (2017).
[19] R. Dutta, H. Thoma, A. Sazonov, B. Náfrádi, M. Meven, A. Gukasov, V. Kocsis, U. Zeitler, A. Puri, Y. Tokunaga, Y. Taguchi, Y. Tokura, S. Bordács, I. Kézsmárki, and V. Hutanu, Phys. Rev. B **107**, 014420 (2023).

[20] S. Mühlbauer, S. Gvasaliya, E. Ressouche, E. Pomjakushina, and A. Zheludev, Phys. Rev. B **86**, 024417 (2012).
[21] H. Murakawa, Y. Onose, S. Miyahara, N. Furukawa, and Y. Tokura, Phys. Rev. Lett. **105**, 137202 (2010).
[22] S. Bordács, I. Kézsmárki, D. Szaller, L. Demkó, N. Kida, H. Murakawa, Y. Onose, R. Shimano, T. Rõõm, U. Nagel, S. Miyahara, N. Furukawa, and Y. Tokura, Nat. Phys. **8**, 734 (2012).
[23] J. W. Kim, S. Khim, S. H. Chun, Y. Jo, L. Balicas, H. T. Yi, S.-W. Cheong, N. Harrison, C. D. Batista, J. Hoon Han, and K. Hoon Kim, Nat. Commun. **5**, 4419 (2014).
[24] S. Toyoda, J.-C. Liao, G.-Y. Guo, Y. Tokunaga, T.-h. Arima, Y. Tokura, and N. Ogawa, Phys. Rev. Mater. **7**, 024403 (2023).
[25] M. Kawano, Y. Onose, and C. Hotta, Commun. Phys. **2**, 27 (2019).
[26] T. Endo, Y. Doi, Y. Hinatsu, and K. Ohoyama, Inorg. Chem. **51**, 3572 (2012).
[27] M. Sale, Q. Xia, M. Avdeev, and C. D. Ling, Inorg. Chem. **58**, 4164 (2019).
[28] A. Sazonov, V. Hutanu, M. Meven, G. Rothand, R. Georgii, T. Masuda, and B. Naáfraádi, Inorg. Chem. **57**, 5089 (2018).
[29] S. Hasegawa, S. Hayashida, S. Asai, M. Matsuura, Z. Igor, and T. Masuda, Phys. Rev. Res. **3**, L032023 (2021).
[30] A. Sazonov, H. Thoma, R. Dutta, M. Meven, A. Gukasov, R. Fittipaldi, V. Granata, T. Masuda, B. Naáfraádi, and V. Hutanu, Phys. Rev. B **108**, 094412 (2023).
[31] M. Soda, M. Matsumoto, M. Månsson, S. Ohira-Kawamura, K. Nakajima, R. Shiina, and T. Masuda, Phys. Rev. Lett. **112**, 127205 (2014).
[32] M. Soda, L.-J. Chang, M. Matsumoto, V. O. Garlea, B. Roessli, J. S. White, H. Kawano-Furukawa, and T. Masuda, Phys. Rev. B **97**, 214437 (2018).
[33] T. Masuda, S. Kitaoka, S. Takamizawa, N. Metoki, K. Kaneko, K. C. Rule, K. Kiefer, H. Manaka, and H. Nojiri, Phys. Rev. B **81**, 100402(R) (2010).
[34] T. Endo, Y. Doi, M. Wakeshima, and Y. Hinatsu, Inorg. Chem. **49**, 10809 (2010).
[35] M. Akaki, T. Tadokoro, H. Kuwahara, T. Kihara, and M. Tokunaga, J. Korean Phys. Soc. **62**, 1812 (2013).
[36] Y. Nambu, M. Kawamata, X. Pang, H. Murakawa, M. Avdeev, H. Kimura, H. Masuda, N. Hanasaki, and Y. Onose, Acta Cryst. B **80**, 393 (2024).
[37] K. Nakajima, S. Ohira-Kawamura, T. Kikuchi, M. Nakamura, R. Kajimoto, Y. Inamura, N. Takahashi, K. Aizawa, K. Suzuya, K. Shibata, T. Nakatani, K. Soyama, R. Maruyama, H. Tanaka, W. Kambara, T. Iwahashi, Y. Itoh, T. Osakabe, S. Wakimoto, K. Kakurai *et al.*, J. Phys. Soc. Jpn. **80**, SB028 (2011).
[38] V. F. Sears, Neutron News **3**, 26 (1992).
[39] J. Kennedy and R. Eberhart, Proc. IEEE Int. Conf. Neural. Netw. **4**, 1942 (1995).
[40] H.-J. Koo, Solid State Commun. **152**, 1116 (2012).
[41] M. Kawano and C. Hotta, Phys. Rev. B **99**, 054422 (2019).
[42] H. Thoma, R. Dutta, V. Hutanu, V. Granata, R. Fittipaldi, Q. Zhang, J. W. Lynn, P. Čermák, N. Khan, S. Nandi, and M. Angst, npj Quantum Mater. **9**, 58 (2024).
[43] T.-H. Jang, S.-H. Do, M. Lee, H. Wu, C. M. Brown, A. D. Christianson, S.-W. Cheong, and J.-H. Park, Phys. Rev. B **104**, 214434 (2021).
[44] S.-H. Do, H. Zhang, D. A. Dahlbom, T. J. Williams, V. O. Garlea, T. Hong, T.-H. Jang, S.-W. Cheong, J.-H. Park, K. Barros, C. D. Batista, and A. D. Christianson, npj Quantum Mater. **8**, 5 (2023).
[45] J. B. Goodenough, Phys. Rev. **100**, 564 (1955).
[46] J. Kanamori, J. Phys. Chem. Solids **10**, 87 (1959).